Brain Inspired Cognitive Systems
August 29 – September 1, 2004
University of Stirling, Scotland, UK

SILICON-BASED NEUROMORPHIC OLFACTORY PATHWAY IMPLEMENTATION

Tim C. Pearce, Department of Engineering, University of Leicester, University Road, Leicester LE1 7RH, United Kingdom. t.c.pearce@le.ac.uk.

Thomas J. Koickal[b], Carlo Fulvi-Mari[a], James A. Covington[c], Forest S. Tan[c], Julian W. Gardner[c], Alister Hamilton[b]

a) Department of Engineering, University of Leicester, University Road, Leicester LE1 7RH, United Kingdom. cfm5@le.ac.uk
b) School of Electronics and Engineering, The King's Buildings, Mayfield Road, Edinburgh EH9 3JL, United Kingdom. {thomas.koickal, alister.hamilton}@ee.ed.ac.uk
c) School of Engineering, University of Warwick, Coventry CV4 7AL, United Kingdom. {su.tan, james.covington, j.w.gardner}@warwick.ac.uk

ABSTRACT

This paper describes our efforts to implement the world's first silicon olfactory system in aVLSI/MEMs. To achieve this requires integration of a biologically constained neuronal model, chemical micro-sensor technology and aVLSI spiking neuromorphic circuits. Here we describe our progress towards this goal, by presenting an olfactory bulb model, a reduced 70 element broadly-tuned chemosensor array (25 different chem-sensor tunings), and details of their silicon implementation. Current results shown here demonstrate that the olfactory bulb model that has been implemented is capable of pattern classification, that the odour delivery, uptake and sensor circuitry, as well as the fundamental units of the neuromorphic model (spike-driven synapse and spiking soma) are all functional. Work will continue towards completing a fully-integrated scalable implementation of the olfactory system.

1. INTRODUCTION

To date neuromorphic silicon implementations of auditory and visual sensory pathways have been undertaken which are in varying states of development [1-3]. Due perhaps to the significant technical challenges involved, and the only recent upsurge of interest, in machine olfaction there have been no reports of equivalent implementations of the olfactory pathway. Although electronic nose technologies exist that have parallels with the biological olfactory pathway (such as exploiting population coding of sensory stimuli), these are in all cases far away from the neuromorphic approach of deploying biologically derived analogue circuitry (in particular spiking neuronal systems) in silicon [4].

Before building such an ambitious system, a key question we should ask is what should such an integrated neuromorphic olfactory system be capable of? Most animals rely on olfactory cues far more than humans - olfaction is fundamental to many animal behaviours, for example, foraging, conspecific mate location, predator avoidance and crypsis (through chemical camouflage). These behaviours rely upon common olfactory detection tasks, which are regularly performed in complex, nonstationary and unpredictable environments. These include:

1. Discrimination between learnt single and multiple compound (simple and complex) odours,
2. identification of specific learnt odours in a background of undefined interfering (and possibly time varying) chemical compounds,
3. separation of odour sources into Gestalts which can be segmented simultaneously, similar to its counterpart in vision – related to binding hypotheses[5], and audition – the so-called cocktail party problem [6].

While portable chemosensor detectors are able to perform routinely the first of these olfactory detection tasks (subject to suitably high chemical concentrations) they cannot reach the performance of an animal, inasmuch as the last two detection problems have not yet been solved technologically. For this reason we aim to exploit what is known about the neuronal architecture of the early olfactory pathway in order to improve technologies for, as well as understand more about biology's solution to, complex chemical detection.

We describe in Sections 2-4 the subsystems upon which this olfactory pathway implementation is based; including a spiking neuronal model of the olfactory bulb, broadly-tuned chemosensor array with associated interface circuitry, and neuromorphic a VLSI circuitry.

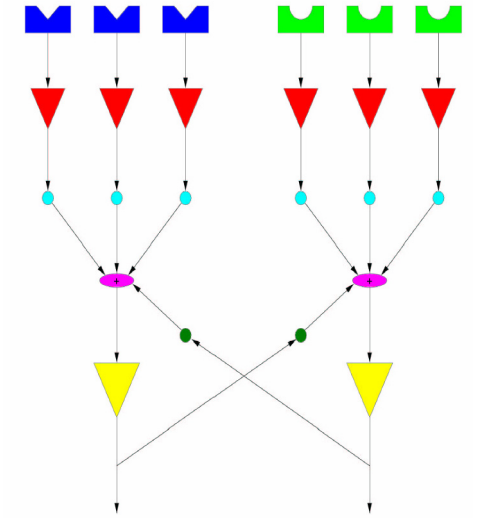

a)

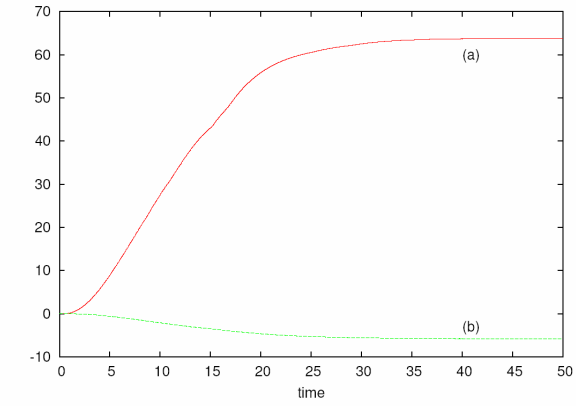

b)

Figure 1 a) A schematic diagram of the olfactory bulb neuronal model architecture, showing receptor and principal neurons (triangles) and synapses (circles), and b) model response in the learnt (red) and naïve (green) stimulus conditions.

2. COMBINED RECEPTOR INPUT AND OLFACTORY BULB NEURONAL MODEL

In Vertebrates, a large number of olfactory receptor neurons (ORNs) constitute the front-end of the olfactory system, being responsible for detecting airborne molecules. Cilia of the ORNs protrude into the olfactory mucosa, where they come in contact with molecules that are transported by the nasal air flow. On the surface of the cilia, odorant receptors bind odorant molecules with a broadly tuned affinity. When a receptor binds with an odorant molecule, it triggers in its ORN a biochemical cascade that eventually causes the membrane potential of the ORN to change, potentially leading to the generation of spikes. Each ORN only expresses one type of odorant receptor, while each type of receptor is usually expressed by a large number of ORNs; for example, in mice around 1,000 types of receptors are expressed by millions of ORNs [7].

ORNs project their axons into the olfactory bulb, terminating into spherical neuropils called glomeruli, where they synapse onto the dendrites of mitral and tufted (M/T) cells. Experimental data indicates that each glomerulus receives the axons of only ORNs that express the same type of receptor, while any M/T cell sends its apical dendrite into one glomerulus only. Inhibitory neurons of the olfactory bulb form reciprocal contacts with many M/T cells, thus forming together a complex network that appears to constitute the first stage of olfactory information processing. The output of the M/T cells is also relayed to higher brain areas [7].

The neural network model here designed is inspired by the olfactory system of vertebrates. The only external signals that the network receives come from the chemosensors (see Section 3), which are responsible for transforming the molecular information of the odorant into signals suitable to constitute neural input. About 25 types of chemosensors, broadly tuned to different chemicals, are expected to be available for the final silicon implementation.

Figure 1a shows the diagram of part of the network, only including two types of sensors for the sake of clarity. The diagram has been drawn representing every computational element with an individual device, rather than adopting a biologically realistic representation. The chemosensors are represented by irregular polygons at the top of the diagram; polygons of the same shape represent sensors of the same type.

There are two classes of neurons, the Receptor Neurons (RNs) and the Principal Neurons (PNs), respectively the smaller and the larger triangles in Figure 1a, that represent, respectively, olfactory receptor neurons and M/T cells. Any RN receives input from one only sensor, and any sensor only projects to one RN. The outputs of the RNs feed into the respective RN-PN synapses (circles). The outputs of the synapses that receive input from RNs fed in by sensors of the same type converge to a summation component (ellipse), where they are summed linearly. The output of any summation component feeds in one respective PN. Because the signals from sensors of the same type are fed forward through neural elements to one and one only PN, the network presents an evident modular structure, each module being defined by a different type of sensor, in a way that resembles the glomerular organization of the olfactory bulb [7]. Every PN projects to every other PN through one of the PN-PN synapses (circles).

The neurons are modelled as integrate-and-fire (IF) units. Below the threshold V_θ, the dynamics of the "membrane" potential $V(t)$ of the IF neuron are defined by the equation

$$\frac{dV(t)}{dt} = -\frac{V(t)}{RC} + \frac{I(t)}{C}$$

a)

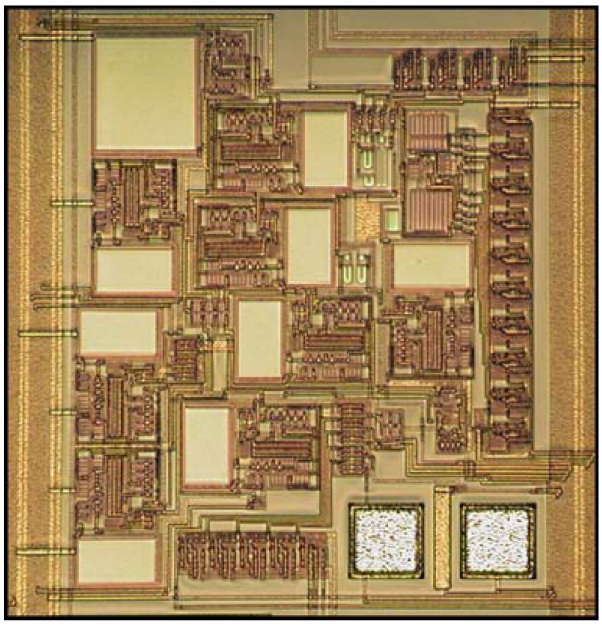

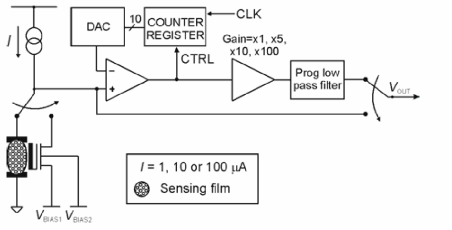

b)

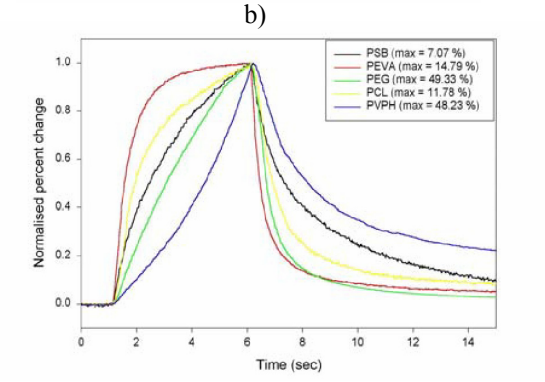

c)

Figure 2 a) footprint of the chemosensor array implementation, b) offset cancellation circuitry, c) representative chemosensor responses, (reproduced from Covington *et al.,* 2004 [9])

where t is time, R and C are, respectively, the membrane resistance and capacitance, and $I(t)$ is the total input current to the neuron. The membrane rest potential is conventionally set equal to 0 V. The membrane time-constant is defined as $\tau_m = RC$. The terms contributing to $I(t)$ are due to sensor responses if the neuron is a RN, and to RNs and lateral interactions if the neuron is a PN. If the potential $V(t)$ reaches the threshold value V_θ, it is immediately reset to the afterhyperpolarization value V_{ahp} and a spike is produced as output of the neuron. The emission of any spike is followed by a refractory time, τ_{refr}, during which the neuron cannot fire but still integrates the input currents.

When a spike reaches a synapse, it triggers the output of a current that is fed into the post-synaptic neuron and that decays exponentially with a characteristic time-constant, starting from a peak value determined by the synaptic weight. The sign of the current is formally included into the synaptic weight, positive or negative according to whether the interaction is, respectively, excitatory or inhibitory. The currents induced by several pre-synaptic spikes add up linearly. If a neuron receives the outputs of several synapses, the respective contributions to the total post-synaptic current add up linearly. The total post-synaptic current constitutes the term $I(t)$ in the equation of the membrane potential of the respective neuron.

The weights of the PN-PN synapses are defined so as to endow the network with associative properties (cf., e.g, [8] for general definitions), though it is not known whether the biological counterpart does perform this kind of processing. The network learns odorants by modifying the weights of the PN-PN synapses according to a one-shot Hebbian learning rule, during a training stage. Given any learnt odorant, a function of the firing rates of the PNs is defined that indicates whether the network output is currently representing that odorant; if a learnt odorant is delivered, then the corresponding indicator function should assume a relatively large positive value. As an example, Fig. 1b shows this function in a simulation of the IF network with 25 sensor types that has already learnt one odorant. The stimulus is currently delivered simultaneously to all the sensors as a step-function of time, starting at zero (time is in units of the PN time-constant, while the y-axis is in arbitrary units); in one case (a) the odorant present in the stimulus is the one previously learnt, while in the other case (b) an unknown odorant is delivered. It is clearly possible to discriminate between recognition and non-recognition cases.

The small size of the repertoire of sensor types presently available, however, can cause the behaviour of the network to vary with different odorants to an extent that normally depends on the complexity of the olfactory task.

3. CHEMOSENSOR ARRAY

Input to our olfactory bulb model is provided by a combined chemFET/resistive sensor array fabricated using an AMS 0.6 μm CUP CMOS process, employing carbon black (CB) composite materials, with integrated signal processing circuitry. It differs from previous work in a number of ways. Firstly, it is the first resistive CMOS compatible sensor array integrating different CB's polymers into the same array. In addition, it is the largest FET sensor array using CB materials. Lastly, it is the first time both a chemoresistor and chemFET have been combined with integrated signal processing electronics.

Combined sensor concept – the resistive sensor component is simply formed by depositing CB polymer material between two sensor electrodes. The FET section is based on a floating gate concept, were the sensing material is capacitive coupled to the floating gate of a FET. As the gate is floating, any potential created through the interaction of the sensing material with the target gas or vapour appears, due to this coupling, on the gate of the FET. It has previously been reported [10] that this is due to a change of workfunction within the sensing material. The

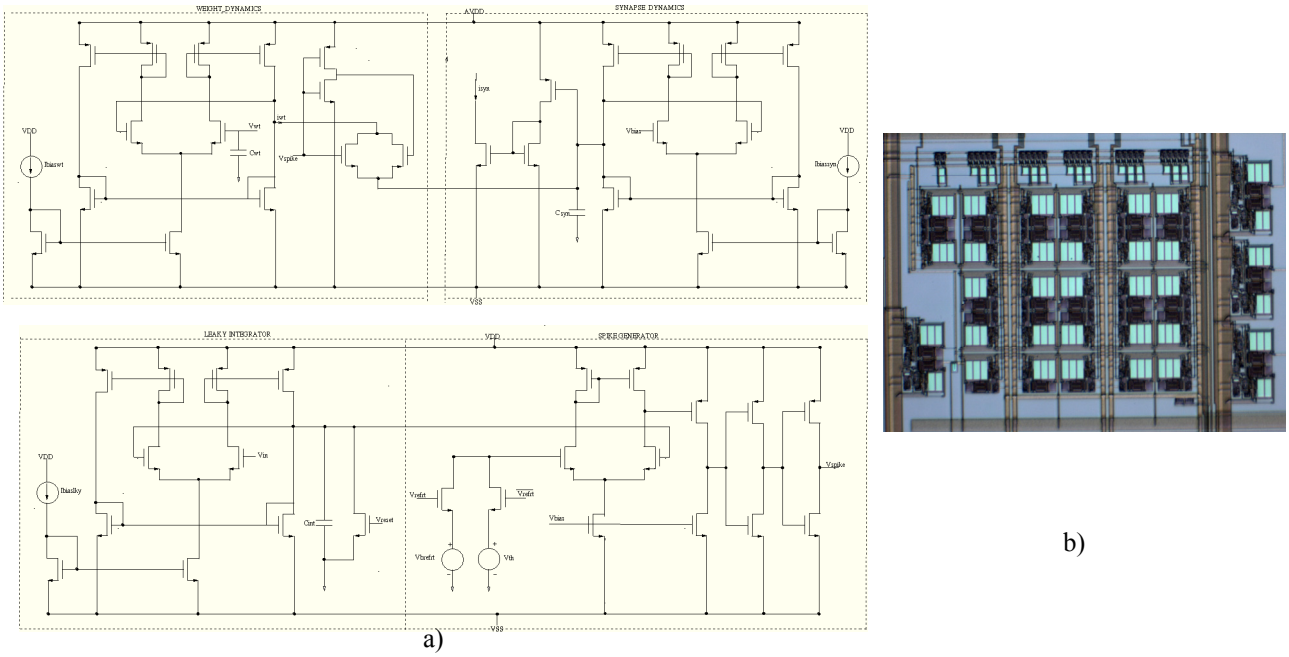

a)

b)

Figure 3 a) Neuromorphic synapse and soma circuit, and b) footprint of the neuromorphic circuit implementation.

floating gate will have an absolute potential subject to variations in the fabrication process. A biasing plate is added underneath the sensing plate and biased to ensure the transistor is turned-on. The capacitive plate is placed in-between the two resistive electrode elements, hence the same sensing material is used for both resistive and FET measurements.

Integrated circuitry - included with each sensor is circuitry to drive and process any response. Each resistive/chemFET sensor is driven by a constant current source and can have three different val-ues (1 μA, 10 μA and 100 μA). This is used to compensate for variations in resistance with different coatings. To re-move the DC baseline value of the sensor, an offset can-

Table 1: Polymer materials used.

Type	Polymer material
1	Poly (styrene-co-butadiene), PSB
2	Poly (ethylene glycol), PEG
3	Poly (Ethyl-co-vinyl acetate), PEVA
4	Poly (4-vinyl phenol), PVPH
5	Poly (caprolactone), PCL

cellation circuit has been added to the design. The circuit allows high gain values to be used without saturating the output. In our design, the DC offset cancellation circuitry uses a ramping DAC with a comparator. The 10-bit DAC ramps to estimate the offset voltage and the value maintained in an internal counter register. The ±1 bit error is only 5 mV and takes only 512 μs (based on 2 MHz clock) to perform a cycle of scanning the offset voltage as all cells are performed in parallel. This baseline removal can be done either before exposure to a vapour or in-situ. Hence, any long term drift of the sensor or changes in environ-mental conditions that alter the DC baseline can be compensated for. Once the baseline has been removed the signal is amplified with gains of 1, 5, 10 or 100. These values are programmed externally and can be altered whilst a test is running. Lastly, the signal is conditioned with a low pass filter set at a corner frequency of 1 kHz. The output voltage is at present measured externally using a data acquisition card. The control bits for each cell are contained within 4 D-type flip-flops and are loaded from an external source. A simplified schematic of the offset removal circuitry is given in Figure 2b.

The sensor array was designed and implemented in the AMS 0.6 μm CUP process and has been tiled across the whole chip. Figure 2a shows a photograph of one cell of the fabricated chip, whilst a close-up of the combined resistor/FET component in shown in Figure 2b. Before CB polymer deposition, the aluminium electrodes have been gold plated. This is to ensure a stable contact between the CB polymer and the aluminium. Five different CB polymers were used as given in Table 1.

The sensitivity for example of the PSB sensor material to ethanol vapour is about 0.00012 %/ppm and 0.00644 %/ppm to toluene vapour. We have also tested other sensors with different coatings to ethanol vapour in air and the results are shown in Figure 2c. Here the sensor array is exposed to a 5 s ethanol vapour pulse at a flow rate of 25 m*l* min^{-1}. The results show that different types of polymer films provide different response profiles (magnitude and response time), thus providing added discriminatory information.

4. NEURONAL MODEL SILICON IMPLEMENTATION

The analogue circuit implementation of the synapse circuit corresponding the circle elements in Figure 1a is shown in Figure 3a (top). The input spike V_{spike} triggers the injection of a current i_{wt} to the capacitor C_{SYN}. The output of the synapse is an expo-

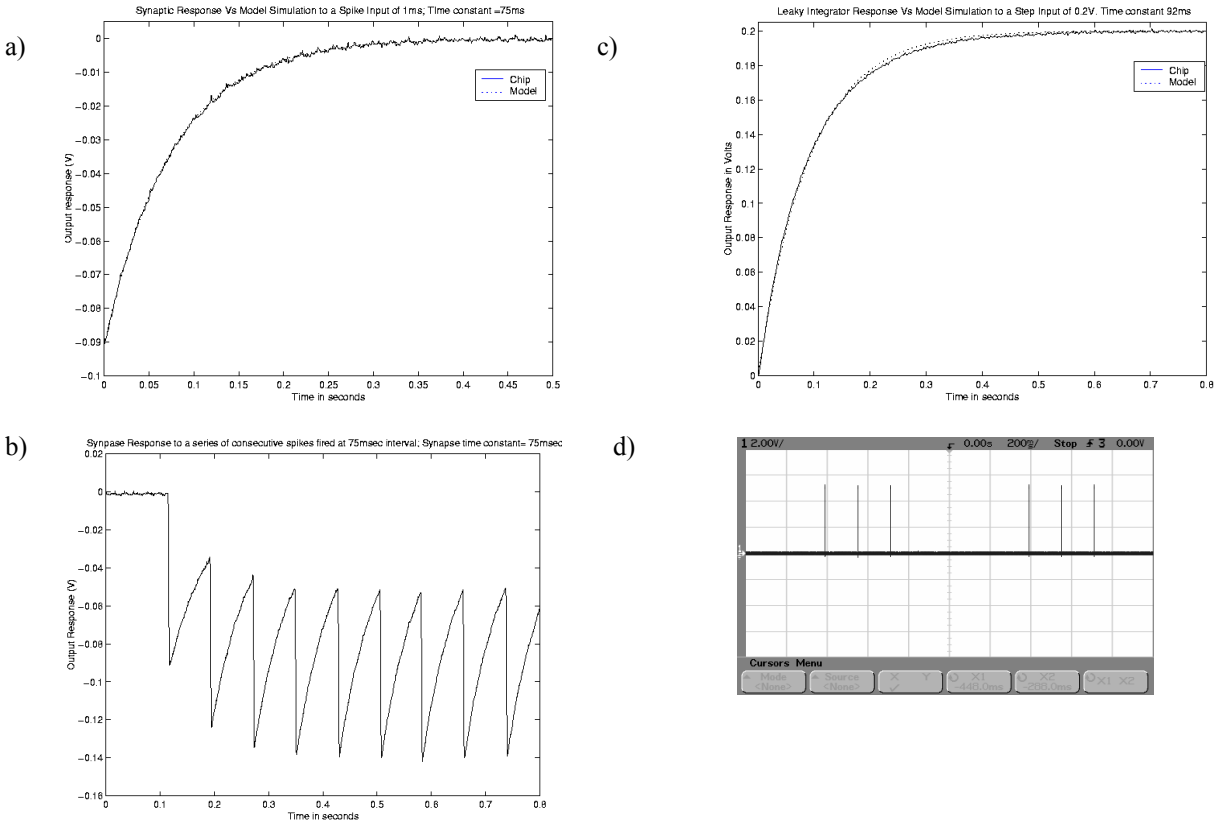

Figure 4) representative circuit behaviour of a) single spike synapse response, b) multiple spike synapse response, c) soma.

nentially decaying current given by i_{syn}. The time constant during the discharging phase is controlled through varying $I_{BIASSYN}$. The weights are stored in capacitor C_{WT} and are updated using a combination of shift registers and switches (not shown in figure).

The analogue VLSI implementation of the spiking neuron has the following functional blocks. They are a) leaky integrator, b) comparator and spike conditioner, and c) reset and refractory timer. The analog circuit implementation of the integrate and fire block is shown in Figure 3a (bottom). The leaky integrator is designed using a operational transconductance amplifier-capacitor (OTA-C) configuration. The output of the integrator is fed to a spike generator circuit. The spike generator circuit consists of a two stage comparator with hysteresis followed by inverters. The reset and refractory period timers are implemented using separate OTA-C circuits (not shown in Figure). V_{reset} and V_{refrt} signals are the output control signals of the reset and refractory period circuits respectively.

Initially the V_{reset} and V_{refrt} signals are at a low state. The output of the comparator V_{spike} goes high when the integrator response is above the threshold voltage V_{th}. The output of the comparator is fed to a reset timer circuit. The reset timer output V_{reset} goes high after a finite interval of time which in turn resets the integrating capacitor C_{int}. The time delay of the reset timer circuit determines the pulse width of the neuron spike output V_{spike} and is externally programmable. The trailing edge of the pulse triggers the refractory timer V_{refrt} to a high state. V_{refrt} signal switches the comparator threshold to a large voltage V_{brefrt} thereby inhibiting the neuron from firing. However, the leaky integrator continues to integrate during the refractory period.

The analogue VLSI implementation of the neuromorphic chip has also been fabricated in AMS 0.6µm CUP process. The chip contains 3 spiking neural network models with each model having 3 RNs, 27 synapses and 1 PN as per the architecture described in Section 2, and is shown in Figure 3b. The network architecture of chip is designed such that a scalable spiking network can be developed through interconnecting multiple chips. The spiking neurons have programmable time constant, refractory period, threshold and spike width. The synaptic circuits have individually programmable weights and are stored on chip. The die area of the chip is 31.5 mm^2. The testing of the chip is currently in progress and the test results of the synapse and neuron circuits on chip are discussed here.

The synapse circuit was tested by exciting it with a spike input with 1 ms duration. The response of the synapse programmed for a weight input of -0.5V and time constant of 75 ms is shown in Figure 4a. Since the sign of the weight is negative with respect to the baseline, the synapse exhibits an inhibitory response. The response is matched with the synaptic model described in Section 2. It is seen that the chip response closely matches the simulated model.

The response of the synapse to consecutive input spikes are given in Figure 4b Series of 10 consecutive spikes of 1msec duration are fired with a time interval of 75 ms. The synaptic weight input is set at -0.5V and the time constant is 75 ms.

The neuron testing was carried out by characterizing the response of the leaky integrator seperately followed by testing the full spiking neuron circuit. The step response of the leaky integrator on chip is shown in Figure 4c. The response is matched with simulated response as the model described in Section 2. To evaluate the working of the whole spiking neuron circuit, a receptor neuron on the 3-27-1 spiking neural network is tested using a square wave input with an amplitude of 0.2 V and period of 1 s. The comparator threshold V_{th} is set at +0.18 V with reference to the baseline output of the leaky integrator. Figure 4d shows the neuron firing for a time constant of 150 ms.

5. CONCLUSIONS & OUTLOOK

We have presented details of the component subsystems of the first aVLSI implementation of the olfactory pathway. These components appear to work correctly, independent of one another and so work will continue to test their combined behaviour in olfactory detection tasks.

One of the key challenges that we face in creating a fully integrated solution is the role of time in the system – which is also one of the most interesting aspects of this endeavour. While chemosensors typically operate on the hundreds of ms scale, aVLSI is naturally suited for far higher bandwidths and so there is great potential for mismatch in the dynamics of the sensor and neuronal model. Large time constants in the aVLSI typically mean large capacitances requiring significant space on the silicon. Solutions exist in the form of multiplexing or buffering between the front-end of the system and the neuronal model, deploying ultra-fast sensors or slowing down the silicon. Time also plays a critical role in terms of the performance of the system. Indeed, a key question we have been addressing is how can the neuronal model we have implemented exploit temporal information in the sensor responses in order to improve detection performance.

ACKNOWLEDGMENTS

This project was funded by the EPSRC (grants GR/ R37968/01 - to TCP, GR/R37975/01 - to JWG, and GR/R37982/01 - to AH).

REFERENCES

[1] Mead C., Analog VLSI and Neural Systems, Addison Wesley, 1989.

[2] Van Torre S., Neuromorphic Systems Engineering: Neural Networks in Silicon, Kluwer, 1998

[3] Liu S-S., Kramer J., Indiveri G., Delbrück T., Douglas R., Analog VLSI: Circuits and Principles, MIT Press, 2002.

[4] Pearce T.C. Schiffman S.S., Nagle H.T., Gardner J.W., Handbook of Machine Olfaction, Wiley-VCH, 2003.

[5] v.d. Malsberg, C., Binding in models of perception and brain function. *Current Opinion in Neurobiology,* **5**, 520-526 (1995).

[6] Cherry E.C., Some experiments in the recognition of speech, with one and two ears. *Journal of the Acoustical Society of America*, **25**, 975-979 (1953).

[7] Mori, K., Nagao H. and Yoshihara Y., The olfactory bulb: coding and processing of odor molecule information, *Science* **286**, 711 (1999).

[8] Amit, D.J., Modelling Brain Function, Cambridge University Press, 1989.

[9] Covington J.A, Tan S.L., Gardner J.W., Hamilton A., Koickal T., Pearce T.C., Combined smart chemFET/resistive sensor array, IEEE Sensor Conference (2003).

[10] Paris R., Pawel S., Herzer T., Doll T., Kornetsky P., Gupta R.P., Eranna G, IEEE Sensor Conference (2002) 421-425.